Optics Letters

Nanovibration detection based on a microsphere

Chunlei Jiang,[1] Weicheng Wang,[1] Bing Yan,[2,3] Peng Chen,[1] Kaichuan Xu,[1] Yu Sun,[1] Zhicheng Cong,[1] Taiji Dong,[1] Yekun Zhou,[1] Zengbo Wang,[2] and Xiufang Wang[1,*]

[1]College of Electrical and Information Engineering, Northeast Petroleum University, Daqing 163318, China
[2]School of Computer Science and Electronic Engineering, Bangor University, Dean Street, Bangor, Gwynedd, LL571UT, UK
[3]Center of Optics Health, Suzhou Institute of Biomedical Engineering and Technology, Chinese Academy of Sciences, No. 88 Keling Street, Suzhou Jiangsu, 215163, China
*Corresponding author: wxfdqpi@163.com

Received 26 May 2022; revised 6 August 2022; accepted 7 August 2022; posted 11 August 2022; published 31 August 2022

We propose a novel, to the best of our knowledge, sensor for nanovibration detection based on a microsphere. The sensor consists of a stretched single-mode fiber and a 2 μm microsphere. The light from the optical fiber passes through the microsphere, forming a photonic nanojet (PNJ) phenomenon at the front of the microsphere. The evanescent field in the PNJ enhances the light reflected from the measured object to the single-mode fiber-microsphere probe (SMFMP). Results showed that the system can detect arbitrary nanovibration waveforms in real time with an SMFMP detection resolution of 1 nm. The voltage signal received and the vibration amplitude showed a good linear relationship within the range of 0–100 nm, with a sensitivity of 0.7 mV/nm and a linearity of more than 99%. The sensor is expected to have potential applications in the field of cell nanovibration detection.

https://doi.org/10.1364/OL.464848

Cell detection technology has been paid increasing attention with the rapid development of biology and medical technology. Evidence shows that cell vibration can reflect the life activities of cells [1]. Therefore, cell life activity can be judged by the real-time monitoring of cell nanovibration.

Atomic force microscopy (AFM) is used to study cell vibrations owing to its high spatial resolution. For contact AFM, the tip is in contact with the surface of the sample, potentially damaging cells. Therefore, in AFM, non-contact (NC) mode is used to avoid this problem [1]. NC mode includes two modes of operation: amplitude modulation mode (AM-AFM) [2] and frequency modulation mode (FM-AFM) [3]. In AM-AFM, the change in oscillation amplitude does not happen immediately: it has a time delay; thus, the scanning speed is very slow. FM-AFM is a detection method suitable for use in an ultrahigh vacuum environment, which also limits the wide application of NC-AFM [3]. In addition, microcantilevers, an extension of AFM, have been used to study tiny fluctuations and cell viability in bacteria, yeast, and eukaryotic cells [4–6]. It can detect dynamic changes in cellular forces, but cantilever functionalization increases the complexity and difficulty of the experiment. Compared with expensive and difficult to manipulate AFM, a series of studies have experimentally demonstrated that optically trapped nanoparticles are capable of detecting nanoscale vibrations as sound or fluid flows when placed in close proximity to a vibrating particle source or flagellated bacteria [7,8]. Although optical tweezer technology enables non-contact vibration detection, it cannot directly observe cell nanovibration. Therefore, developing a non-contact sensor with a simple design suitable for the real-time detection of cell nanovibration is needed. Microsphere-based sensors provide a simple and sensitive method of detection. At present, microsphere-based fiber optic probes are made by a fusion splicer or CO_2 laser, and are widely used in displacement sensing [9], glucose sensors [10], and strain and temperature sensors [11], etc. We know that a higher refractive index (RI) contrast yields stronger focusing and a narrower photonic nanojet (PNJ), which facilitates the detection of near-field signals [12]. These sensors are limited to optical fiber raw materials. Additionally, the microsphere size is larger than the fiber diameter and it is therefore not regarded as a fiber tip sensor, reducing its sensitivity to nanovibration detection. Some researchers have combined microspheres of different materials with fibers to make probes [13]. However, these sensors have relatively high requirements in the fabrication process, and most of these sensors have a size of tens of microns or even hundreds of microns and are used for temperature and humidity sensing. Sensor miniaturization is particularly important for cell vibration detection. Therefore, the fiber can be drawn very thin and then combined with high-RI microspheres.

In this paper, we present a new type of miniature sensor for nanovibration detection. We stretched a single-mode fiber and combined it with a polystyrene microsphere, which overcomes the limitations of microsphere material and size. The addition of high-RI microspheres resulted in the formation of a PNJ with an evanescent field component at its front, which plays an enhanced role in nanovibration detection. The sensor realizes the real-time detection of the nanovibration of an arbitrary waveform with a detection resolution of 1 nm. It has the advantages of a simple design, easy operation, miniaturization, and being non-contact and low cost. To the best of our knowledge, this work is the first in the current literature to use a microfiber-microsphere probe for the real-time detection of nanovibration waveforms with detection units of several nanometers. This sensor is expected to have potential applications in highly sensitive cell vibration sensors.

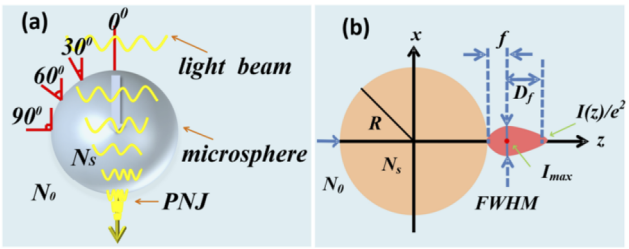

Fig. 1. (a) Schematic of the generation principle of the PNJ. (b) Schematic of the PNJ parameters.

The PNJ generated at the front end of the microsphere can be attributed to the superposition of multi-beam interference. As shown in Fig. 1(a), when the incident light is incident on the microsphere surface, the incident light can be regarded as parallel light. The parallel light forms different incident angles with the spherical surface of the microsphere and refracts into the interior of the microsphere. According to the angular spectrum theory of plane waves, a series of discrete coherent beams are superposed to form a focused beam. This beam is the PNJ. The characteristics of the PNJ can be described by four parameters [Fig. 1(b)]: the focal distance f from the surface of the microsphere to the point of maximum intensity, the intensity enhancement I_{max} at the focus, the full width at half maximum (FWHM) at the focus, and the diffraction length D_f. Higher light intensity, a longer focal length, a smaller FWHM, and a longer effective length will be beneficial for nanovibration detection. The RI of the microsphere is N_S, and that of the surrounding medium is N_0. The index contrast is $\rho = N_S/N_0$. The radius of the microsphere is R. The existence of evanescent fields in the PNJ produced by tiny microspheres with high index contrast has been demonstrated. When the evanescent field is removed, the maximum-intensity position of the PNJ moves away from the surface, the maximum field enhancement drops, and the FWHM is increased [12]. The evanescent field contributions to PNJ created by the microspheres enhance and sharpen the nanovibration detection of near-field surfaces. The distance of the evanescent field beyond the microsphere interface is described by the penetration depth d_p:

$$d_p = \frac{\lambda}{2\pi\sqrt{N_S^2\sin^2\theta - N_0^2}}, \tag{1}$$

where λ is the wavelength of the light source, θ is the angle of incidence of the light at the microsphere and air interface; and N_S and N_0 are the RIs of the microsphere and air, respectively.

The proposed single-mode fiber-microsphere probe (SMFMP) works via the two-beam interference principle, as shown in Fig. 2(a). When the light is injected into the microsphere, a part of it is reflected by the microsphere surface, and some portion passes through the microsphere and is reflected by the vibrating object. This can be expressed as follows:

$$P_r = P_i\left[R_1 + R_2 - 2\sqrt{R_1R_2}\cos\left(4\pi\frac{N_0L}{\lambda}\right)\right], \tag{2}$$

where P_i and P_r are the incident light power and reflected light power, respectively; R_1 and R_2 are the RIs of the two reflecting surfaces; λ is the wavelength of the incident light; N_0 is the RI of air ($N_0 = 1$); and L is the external cavity length ($L = L_0 + \Delta L$). L_0 represents the initial external cavity length and ΔL is the vibration amplitude of the external object. Figure 2(b) shows the output function curve of Eq. (2) (normalized). The abscissa is the length of the cavity, and the ordinate is the reflected light power. Therefore, when the change of external cavity length L is limited to the small range of $\lambda/8$, the reflected light power P_r and the vibration amplitude of the external object ΔL can be approximately expressed as follows:

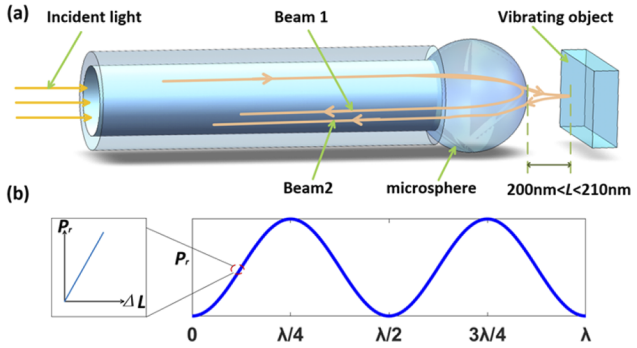

Fig. 2. Principle of nanovibration detection. (a) Schematic of two-beam interference. (b) Function diagram of the reflected light power P_r and external cavity length L.

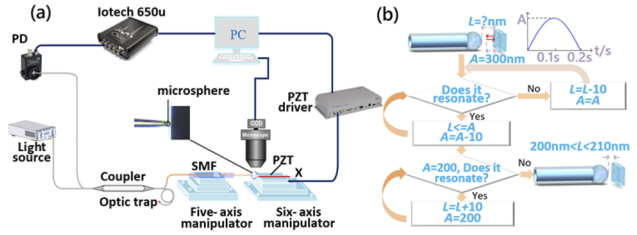

Fig. 3. (a) Schematic of the experimental setup. (b) Flow chart for controlling the distance between probe and PZT.

$$P_r = \alpha\Delta L, \tag{3}$$

where $\alpha = \beta P_i$, and β is the proportional coefficient, a constant value. There is a good linear relationship between the reflected light power and the vibration amplitude of the external object.

The experimental setup is shown in Fig. 3. The light source is provided by a distributed feedback laser with a wavelength of 1550 nm (THORLABS, S1FC1550). The light emitted from the laser is divided into two beams in a ratio of 50/50 through a 2×2 coupler (THORLABS, TN1550R5A2). One beam enters the SMFMP and the other is connected to the optical trap (THORLABS, FTFC1). The vibrating object is a piezoelectric transducer (PZT). The light transmitted to the PZT is returned to the input direction by the coupler and received by the photodetector (PD) collector (THORLABS, DET01CFC) on the other port. Finally, the signals are converted from analog to digital by a data acquisition card (IOtech) and transferred to a PC. We stripped the coating from a single-mode fiber with a core diameter of 9 μm and a cladding diameter of 125 μm. Then, the front end of the fiber was drawn into a 12 μm cone by the hot-melt drawing method. The diameter of the single-mode fiber dropped rapidly from 3 μm to 1 μm at 1.5 μm from the top. We chose to use a polystyrene microsphere of 2 μm diameter. The end face of the single-mode fiber was coated with UV-curable epoxy with a thickness of 100 nm, and then the microsphere was embedded. Finally, we used a UV light-emitting diode (LED)

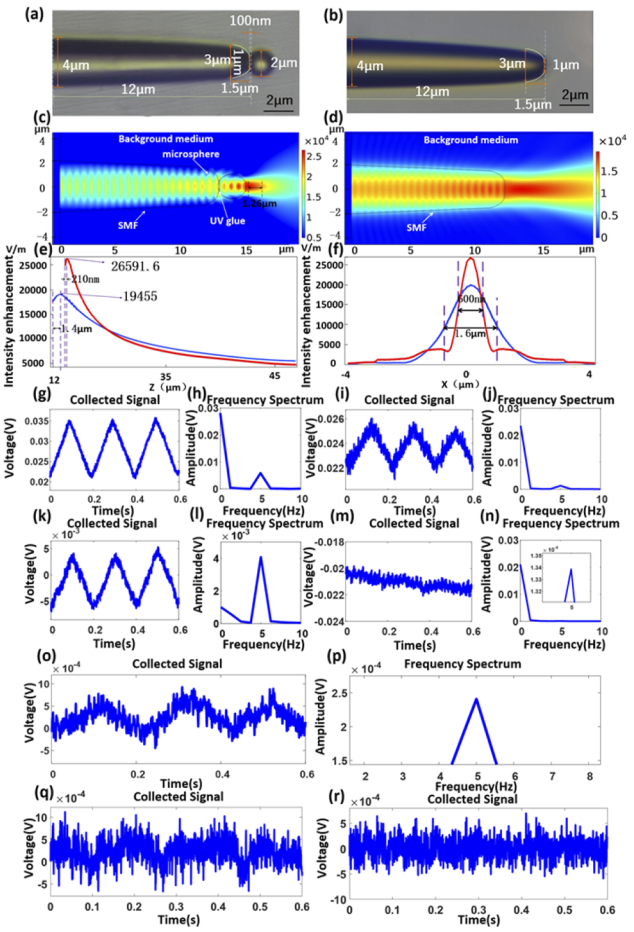

Fig. 4. Probes and vibration signals. (a) SMFMP. (b) SMFP. (c) Simulation of the SMFMP. (d) Simulation of the SMFP. (e) Electric field strength propagating along the propagation axis z; the red and blue curves represent the PNJ intensity along the propagation axis drawn from the front surface of the microsphere of the SMFMF and the single-mode fiber end face. (f) Intensity distribution of the electric field at $z=f$; the red and blue curves represent the transverse intensities of the SMFMP and SMFP. When the PZT was driven to perform a triangle wave, signals were detected by PD. (g) SMFMP, the vibration signal, 20 nm, 5 Hz. (h) SMFMP, the frequency, 20 nm, 5 Hz. (i) SMFMP, the vibration signal, 5 nm, 5 Hz. (j) SMFMP, the frequency, 5 nm, 5 Hz. (k) SMFP, the vibration signal, 20 nm, 5 Hz. (l) SMFP, the frequency, 20 nm, 5 Hz. (m) SMFP, the vibration signal, 5 nm, 5 Hz. (n) SMFP, the frequency, 5 nm, 5 Hz. (o) SMFMP, the vibration signal, 1 nm, 5 Hz. (p) SMFMP, the frequency, 1 nm, 5 Hz. (q) Signals detected at a distance of 500 nm. (r) Signals detected at a distance of 600 nm.

to illuminate the UV-curable epoxy and obtain the SMFMP, as shown in Fig. 4(a). During the experiment, we controlled the distance between the probe and the PZT to 200 nm by vibrating the PZT and observing whether the probe resonated with it. This process is shown in Fig. 3(b), where L is the distance between the probe and the PZT and A is the amplitude of the PZT. "+" means the PZT is stepping closer to the probe, and "-" means the PZT is stepping away from the probe.

We carried out comparative experiments to verify the focusing effect of the microsphere. We performed experiments with the probes, as shown in Fig. 4(a) and 4(b). Figures 4(c) and 4(d) are simulation diagrams of the SMFMP and a single-mode fiber probe (SMFP), respectively. The diameter of the microsphere is 2 μm and the RI is 1.59. The RI of the background medium (air) is 1. The wavelength of the light source is 1550 nm and the power is 2 mW. The red and blue curves in Fig. 4(e) represent the PNJ intensity along the propagation axis drawn from the front surface of the SMFMP and SMFP, respectively. The red and blue curves in Fig. 4(b) represent the transverse intensities of the SMFMP and SMFP, respectively, at $z=f$. Figures 4(e) and 4(f) show that combination with the microsphere shortened the focal length (from 1.4 μm to 210 nm), increased the intensity (from 19455 V/m to 26591.6 V/m), and decreased the FWHM (from 1.6 μm to 600 nm). Then the PZT was driven by a triangular wave with an amplitude of 20 nm and a frequency of 5 Hz. Figures 4(g)–4(h) show the vibration waveform and frequency detected by the SMFMP. Figures 4(k)–4(l) show the signals detected by the SMFP. The vibration waveform and frequency were observed with both probes. However, the peak-to-peak voltage of the signal detected by the SMFMP was 37% higher than that detected by the SMFP. Then the vibration amplitude of the PZT was sequentially reduced. In this process, although the vibration waveform and frequency were detected with the SMFP, they gradually become more difficult to identify. A remarkable difference was observed when the amplitude was reduced to 5 nm. Figures 4(i)–4(j) show the signals detected using the SMFMP, while Figs. 4(m)–4(n) show the signal detected using the SMFP. Evidently, the SMFMP can detect clear waveforms whereas the SMFP cannot. The amplitude of the PZT continued to decrease, and we used the SMFMP to detect. The detection resolution of the SMFMP can reach 1 nm [Figs. 4(o)–4(p)]. We controlled the distance between the SMFMP and the PZT such that it gradually increased, and the vibration waveform became progressively worse [Fig. 4(q)]. When the distance between the probe and the object was about 550 nm, the signal was completely drowned in noise [Fig. 4(r)].

Then the PZT was driven by a triangle wave, sine wave, sawtooth wave, and rectangle wave with an amplitude of 50 nm and a frequency of 5 Hz [Figs. 5(a)–5(d)]. Figures 5(e)–5(l) show the waveform and frequency we collected. The three-period signal was selected to facilitate observation. Evidently, the detected waveform and frequency were consistent with the PZT vibration waveform and frequency.

The nanovibration amplitude of the PZT was changed from 1 nm to 100 nm in intervals of 10 nm. Then, the nanovibration waveform and frequency were detected in real time on the PC. The collected signal was processed, and the peak-to-peak voltage value of the vibration signal was obtained. The relationship between the voltage signal and the vibration amplitude is plotted in Fig. 6. The abscissa represents the vibration amplitude of the PZT, and the ordinate represents the peak-to-peak voltage. The blue dots represent the experimental results collected with different vibration amplitudes. The red curve was obtained by fitting. The results show a good linear relationship between the voltage value of the signal received at the PC and the vibration amplitude of the PZT. The sensitivity was 0.7 mV/nm and the linearity was more than 99%.

The SMFMP was combined with a 2 μm polystyrene microsphere to form a PNJ with a focal length of 210 nm, which is close to the position of the cavity length $\lambda/8$ and has better linearity. Importantly, the evanescent field at the microsphere surface remained at 200–500 nm, which is the basis for improved detection resolution. These conditions played enhancing and sharpening functions in the nanovibration detection process.

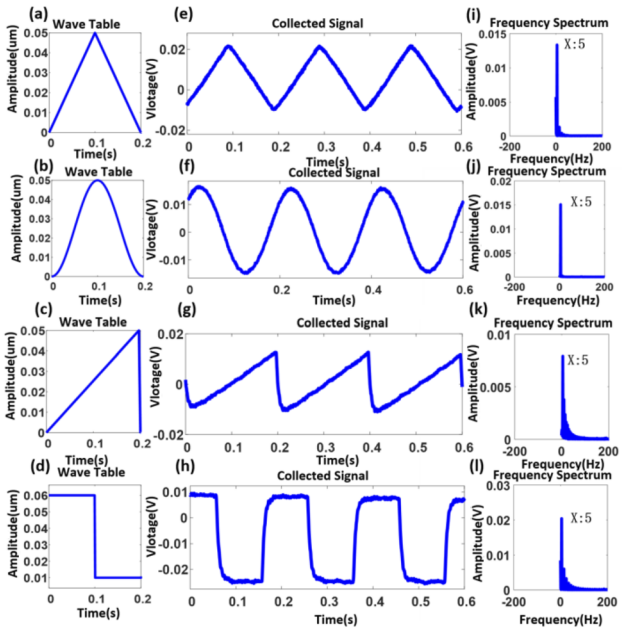

Fig. 5. Signal graph and the spectrogram. The PZT was driven to perform different waveforms with an amplitude of 50 nm and a frequency of 5 Hz. (a)–(d) Vibration waveform of PZT. (e)–(h) Detected waveform. (i)–(l) Detected frequency.

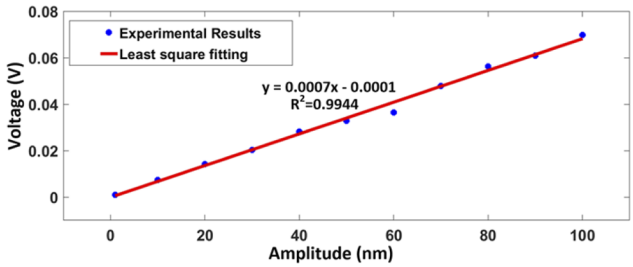

Fig. 6. Relationship between the voltage and the vibration amplitude of the PZT.

The structure of the SMFMP, including the size and material of the microspheres, and the shape of the drawn single-mode fiber affect the properties of the PNJ, the optimal distance between the SMFMP and the vibrating object, and the sensitivity of the sensor. However, the ease of operation, linearity at the location of the strongest light intensity, and the penetration depth of the evanescent field should also be considered in the process of making the probe.

In summary, a miniature fiber sensor based on a microsphere was fabricated and verified by experiments. This sensor can be used to detect nanovibration waveforms and frequencies in real time. The detection resolution of the SMFMP is 1 nm. When the vibration amplitude is 0–100 nm, the output voltage intensity increases linearly, the sensitivity is 0.7 mV/nm, and the linearity is greater than 99%. The sensor has the advantages of a simple design, miniaturization, high resolution, and being non-contact and low cost. It provides a new method for the real-time monitoring of cells, and will become a new and promising detection technology.

Funding. Natural Science Foundation of Heilongjiang Province (LH2021F008).

Disclosures. The authors declare no conflicts of interest.

Data availability. Data underlying the results presented in this paper are not publicly available at this time but may be obtained from the authors upon reasonable request.

REFERENCES

1. S. L. Nelson, D. T. Proctor, A. Ghasemloonia, S. Lama, K. Zareinia, Y. Ahn, M. R. Al-Saiedy, F. H. Y. Green, M. W. Amrein, and G. R. Sutherland, Theranostics **7**, 2417 (2017).
2. Y. Martin, C. C. Williams, and H. K. Wickramasinghe, J. Appl. Phys. **61**, 4723 (1987).
3. T. R. Albrecht, P. Grütter, D. Horne, and D. Rugar, J. Appl. Phys. **69**, 668 (1991).
4. S. Kasas, F. S. Ruggeri, C. Benadiba, C. Maillard, P. Stupar, H. Tournu, G. Dietler, and G. Longo, Proc. Natl. Acad. Sci. U. S. A. **112**, 378 (2015).
5. S. Wu, X. Liu, X. Zhou, X. M. Liang, D. Gao, H. Liu, G. Zhao, Q. Zhang, and X. Wu, Biosens. Bioelectron. **77**, 164 (2016).
6. C. Lissandrello, F. Inci, M. Francom, M. R. Paul, U. Demirci, and K. L. Ekinci, Appl. Phys. Lett. **105**, 113701 (2014).
7. S. R. Kirchner, S. Nedev, S. Carretero-Palacios, A. Mader, M. Opitz, T. Lohmüller, and J. Feldmann, Appl. Phys. Lett. **104**, 093701 (2014).
8. A. Ohlinger, A. Deak, A. A. Lutich, and J. Feldmann, Phys. Rev. Lett. **108**, 018101 (2012).
9. R. Fan, Y. Luo, L. Li, Q. Wu, Z. Ren, and B. Peng, Opt. Fiber Technol. **48**, 173 (2019).
10. S. W. Harun, A. A. Jasim, H. A. Rahman, M. Z. Muhammad, and H. Ahmad, IEEE Sens. J. **13**, 348 (2013).
11. M. S. Ferreira, J. L. Santos, and O. Frazao, Opt. Lett. **39**, 5937 (2014).
12. A. Devilez, B. Stout, N. Bonod, and E. Popov, Opt. Express **16**, 14200 (2008).
13. W. P. Chen, D. N. Wang, B. Xu, Z. K. Wang, and C.-L. Zhao, Opt. Eng. **56**, 057107 (2017).